ARMY RESEARCH LABORATORY

Analysis of the Noneroding Penetration of Tungsten Alloy Long Rods Into Aluminum Targets

by Steven B. Segletes

NOTICES

Disclaimers

The findings in this report are not to be construed as an official Department of the Army position unless so designated by other authorized documents.

Citation of manufacturer's or trade names does not constitute an official endorsement or approval of the use thereof.

Destroy this report when it is no longer needed. Do not return it to the originator.

Army Research Laboratory

Aberdeen Proving Ground, MD 21005-5066

ARL-TR-3075 September 2003

Analysis of the Noneroding Penetration of Tungsten Alloy Long Rods Into Aluminum Targets

Steven B. Segletes
Weapons and Materials Research Directorate, ARL

1. REPORT DATE *(DD-MM-YYYY)*	2. REPORT TYPE	3. DATES COVERED *(From - To)*
September 2003	Final	October 2000 – March 2003

4. TITLE AND SUBTITLE	5a. CONTRACT NUMBER
Analysis of the Noneroding Penetration of Tungsten Alloy Long Rods Into Aluminum Targets	
	5b. GRANT NUMBER
	5c. PROGRAM ELEMENT NUMBER
6. AUTHOR(S)	**5d. PROJECT NUMBER**
Steven B. Segletes	AH80
	5e. TASK NUMBER
	5f. WORK UNIT NUMBER

7. PERFORMING ORGANIZATION NAME(S) AND ADDRESS(ES)	8. PERFORMING ORGANIZATION REPORT NUMBER
U.S. Army Research Laboratory ATTN: AMSRL-WM-TD Aberdeen Proving Ground, MD 21005-5066	ARL-TR-3075

9. SPONSORING/MONITORING AGENCY NAME(S) AND ADDRESS(ES)	10. SPONSOR/MONITOR'S ACRONYM(S)
	11. SPONSOR/MONITOR'S REPORT NUMBER(S)

12. DISTRIBUTION/AVAILABILITY STATEMENT

Approved for public release; distribution is unlimited.

13. SUPPLEMENTARY NOTES

14. ABSTRACT

Data concerning the rigid/eroding-rod threshold transition are reported for hemispherical-nosed tungsten rods penetrating into thick 5083-aluminum targets. Presented data quantitatively buttress existing explanations. The current analysis suggests that the penetrator must bring to bear a different "apparent" strength in the noneroding- vs. the eroding-penetration regimes. Conventional one-dimensional penetration analysis reveals that the noneroding datum is wholly consistent with the notion of treating the rod as if it penetrated in a rigid-body fashion, possessing unrealistically high yield strength. Study of a recovered rod fragment reveals that the penetrating rod nonetheless deformed, but did so without erosion. Such an observation for hemispherical-nosed rods is consistent with past qualitative explanations posited for ogival-nosed rods. The phenomenon, supported by analysis, is that an exaggerated stress was axially applied by the rod to the target interface, composed of both the rod's intrinsic yield strength plus a confining stress caused by a lateral interference fit between the rod and target during the penetration event. The lateral interference of the target was kinematically sufficient to prevent an erosive flow field from being established in the rod. In such a fashion, the rod was able to employ the target's lateral resistance to great axial advantage.

15. SUBJECT TERMS

noneroding, penetration, rigid-body, tungsten, aluminum, analysis

16. SECURITY CLASSIFICATION OF:			17. LIMITATION OF ABSTRACT	18. NUMBER OF PAGES	19a. NAME OF RESPONSIBLE PERSON Steven B. Segletes
a. REPORT	**b. ABSTRACT**	**c. THIS PAGE**			**19b. TELEPHONE NUMBER** *(Include area code)*
UNCLASSIFIED	UNCLASSIFIED	UNCLASSIFIED	UL	42	410-278-1939

Contents

List of Figures

Acknowledgments

Intentionally left blank.

1. Introduction

This report details a ballistic result observed from the impact of a hemispherically capped tungsten alloy rod into a monolithic aluminum-5083 (Al-5083) target. The testing was conducted in the summer of 2001. The data span impact velocities over what is known as the transitional range, between so-called "rigid-body" penetration and eroding-body penetration, and provide corroborative evidence to existing theories on the subject. What makes the data of particular interest is the nature of the noneroding phase of penetration, below the threshold velocity, which was observed as not truly rigid, yet at the same time noneroding. The three tests comprising the presented data were part of a larger test series. This larger test series will be addressed by the author in a separate report (manuscript in preparation), whose focus will not be solely limited to the issue of threshold velocity.

We analyze the data presented here in terms of a one-dimensional penetration model (*1*), itself an adaptation of Tate-Alekseevskii (*2, 3*) and follow-on methodologies (*4–6*). The model (*1*) has previously been employed (*7*) to describe, very successfully, the penetration/perforation behavior of small-caliber (14.5 mm B32) munitions through laminate targets.

The ballistic response in the low-velocity regime is uniquely different from the response in the higher velocity eroding-penetration regime, where most research attention has been directed in recent decades. In the low-velocity regime, interesting behavior has been noted wherein the penetration is observed to exceed the penetration of the identical configuration at higher impact velocities. Kinslow (*8*) noted in the 1960s the disparity between the low-velocity and high-velocity penetration behaviors, particularly for the case of hard-projectile/ductile-target configurations. Brooks and Erikson (*9*) studied the low-velocity regime in 1971 and noted a profound dependence upon both rod-material as well as rod nose-shape, for hard-rod/ductile-target combinations. They noted this unique behavior to be a strong function of the cone angle in conical-nosed rods and found ogival-nosed rods to exhibit this elevated-penetration behavior more profoundly, a response so different from the conical-nosed rods that they deemed the result "anomalous." Their experimental results led them to infer that the ogival rod's "nose is supported hydrostatically by the target material." This observation will be important to the current report, as it attempts to connect the elevated-penetration behavior not only with the nose shape, but also with a multi-axial stress state imposed on the rod by the target.

In 1980, Hill (*10*) recounted his work dating back to World War II. His interest here concerned the nature of penetration prior to and the onset of what he called ballistic "cavitation." Hill defines ballistic cavitation as penetration wherein the crater formed by the penetrating rod becomes larger than the diameter of the rod itself, a kinematic condition later noted by Wijk (*11*) as necessary to permit rod erosion. He understood that noncavitating (thus, noneroding) penetration, associated with lower velocity penetrations, was more efficient than

cavitating penetration, wherein the extreme case "the missile itself deforms and the entire physics is different in kind." Furthermore, the shape of the rod's nose was seen as an overarching factor in the behavior because the nose shape was primarily responsible for determining the velocity at which cavitation might manifest itself. Hill notes that, in noncavitating penetration, the average axial stress (axial load per unit area) in the rod is dependent on "the mean work to form unit volume of the resultant (target) cavity," and not upon the inertial stresses of impact (*i.e.*, those stresses proportional to ρV^2, where ρ is density and V is velocity).

Forrestal *et al.* (*12*), in 1988, formulated a more detailed description of noneroding penetration that accounted for rod's nose shape and, unlike Hill (*10*), included inertial terms in addition to target strength terms in the formulation of the axial stress component. The inertial component of axial stress in the Forrestal model was shown to be proportional to $(V/c)^2$, where c is the bulk sound speed. However, the proportionality constant is such that the contribution of this term to the axial stress is often minor for material combinations and noncavitating impact velocities of interest. In either case, neither Hill nor Forrestal *et al.* address the specific case of current interest, wherein the average axial stress at the rod's nose exceeds the rod's intrinsic strength, even as the penetration remains noneroding. In the same trend, Forrestal's later coauthored works (*13−16*), validating the merit of the 1988 theory, retained impact conditions that specifically sought to exclude rod plasticity.

In contrast, Woodward was very much interested in the low-velocity penetration regime where explicit penetrator plasticity was, nonetheless, evident. His 1980s papers (*17, 18*) focus solely on conical-nosed penetrators, for which he showed the low-velocity penetrating-flow structure to be unique. When the rod angle is not so small, such that the narrow tip bends or buckles outright, there instead occurs a flow separation of crater material from the rod at the location where the conical rod tip merges with the cylindrical rod shank. This flow separation allows the rod shank to strain radially, while the conical tip is simultaneously restrained by the crater. If the impact velocity is large enough, the resulting shear strain at this location causes a shearing fracture in the rod, between the shank and conical nose. Thereafter, the embedded conical tip appears to remain rigid and is pushed through the target by an eroding cylindrical shank that bears down upon it. Woodward noted the penetration capacity to be dependent upon the included angle of the conical rod tip. This cone-angle dependence of penetration capacity can be attributed to the relative ease by which a sharp nose embeds in a target material vis-à-vis a blunt nose. From a traditional one-dimensional penetration analysis point of view, this dependence would, at minimum, show up in the target's k_T "shape factor" parameter of the inertial stress, $k_T \rho_T U^2$, where U is the penetration velocity of the event. Segletes *et al.* (*7*) noted that the functionality of this variation should proceed as $1/2 \cdot (1 - \cos\delta)$, where δ is the half angle of the rigid conical nose of the rod.

While much of the cited investigation through the 1980s was experimental and/or analytical in nature, some more recent efforts have adopted computational approaches to studying the low-velocity penetration regime. In some cases, like that of Chen (*19*), perforation by rigid penetrators was of interest, and so rod plasticity was effectively precluded by modeling the projectile with a

small number of coarsely resolved high-strength elements. Yatteau and Dzwilewski (*20*), in 1995, augmented their experiments with code computations to assist in the analytical modeling of conical-nosed penetrators at low velocity. Their resulting model appears fully consistent with the concepts espoused by Woodward (*17, 18*) on the phenomenology of low-velocity conical-tip rod penetration. Specifically, the model allows for the embedded conical rod tip to fracture from the rod shank and remain rigid while the shank bearing upon it is permitted to erode.

More recently still, Scheffler (*21, 22*) employed computational modeling to examine the noneroding phenomenon for tungsten alloy rods, with ogival and hemispherical nose shapes, upon aluminum targets. Interestingly, Scheffler's stated intent was to test a new computational algorithm in the CTH code (the BLINT, or Boundary Layer INTerface algorithm), intended to provide needed improvements for modeling noneroding penetration. Scheffler's computations with CTH, using BLINT, compared favorably with the experiments of Magness (*23*), which were, to that point, unpublished. Both Magness' data and Scheffler's computations corroborated the unusual penetration behavior that Brooks and Erikson (*9*), decades earlier, had deemed "anomalous." In particular, even as the transition velocity for ogival-nosed rods was significantly higher than that for hemispherical-nosed rods, in both cases the penetration levels just below the erosion-threshold velocity were observed to be significantly more than double that of experiments and computations at striking velocities above this transition velocity. And while Scheffler referred to this type of penetration as "rigid" (rather than noneroding), he nonetheless notes that, in his computations, the rods indeed deformed. In the case of the hemispherical-nosed rods perforating finite plates, Scheffler's computations (*21, 22*) generally revealed an increased diameter near the front of the rod and a significantly flattened nose profile, resulting from the target interaction.

Magness and Scheffler (*23*) most recently addressed this issue in greater detail, for both tungsten alloy and depleted uranium penetrators, and formulated a phenomenology for how the process occurs for ogival-nosed rods, which we will quote at some length. Just below the erosion-threshold velocity, based upon their computations of ogival-nosed penetrators, they describe the penetration phenomenology thus:

> "The rapid [radial] displacement of the armor material initially causes it to lift off the surface of the ogival nose. Penetrator material located immediately behind the contact surface is not confined by armor material and deforms until contact is re-established with the wall of the penetration cavity. This process continues as the projectile burrows into the target. This deformation appears as a high strain-rate region where the shank of the penetrator meets the enlarged head. This high strain-rate region propagates toward the rear of the rod as the penetration continues. Strain rates drop rapidly in the head of the penetrator once it is constrained by the surrounding armor material and loaded under triaxial compression."

3

Above this erosion-threshold transition, as the penetration levels drop, they note that the phenomenology of the ogival-nosed penetration computation seems to follow the phenomenology described by Woodward for conical-nosed penetrators, in which the imbedded penetrator nose is rigidly pushed ahead of an eroding-rod shank. No simulations are presented for the hemispherical-nosed rods, though the data cited for the tungsten alloy hemi-rods appear the same as presented previously by Scheffler (*21*).

Forrestal and Piekutowski (*24*) present much data of a similar character. In their work, 6061-T6511 Al targets are penetrated by hemispherical-nosed steel rods of hardnesses R_C 36.6, 39.5, and 46.2. While the work here employs tungsten alloy (WA) rods, both rod hardness and target hardness were comparable to that employed by Forrestal and Piekutowski. To model their data, they use an eroding model above the erosion threshold and a rigid model below it, in order to recreate the observed penetration discontinuity at the threshold. Forrestal and Piekutowski also note (with radiography of rods embedded in targets) significant rod-bulging deformities below the erosion threshold, which is to say, among those data for which rigid-body modeling was applied. No hypotheses are, however, offered by Forrestal and Piekutowski as to how and why a significantly deforming rod should be treated as "rigid" in an analysis, and more importantly, the kinematic justification for why such a rod fails to erode in the first place. We intend to explore such issues here.

Earlier work of Piekutowski *et al.* (*25*) using nearly identical materials, but ogival instead of hemispherical rods, demonstrates (as have many other authors) the dependence of the transition phenomenon on rod-nose shape. There, the transition to deforming and subsequent rod erosion was only observed at significantly higher striking velocities.

Like Brooks and Erikson (*9*) before them (who noted "hydrostatic" support of the ogival rod nose), Magness and Scheffler (*23*) attribute the presence of a triaxial compression to the phenomenology of ogival-nosed penetration below the erosion-threshold velocity. The work of this report will be to present data that further corroborates these explanations of Brooks and Erikson (*9*) and Magness and Scheffler (*23*), while providing additional information about the deformations and stress states associated with the noneroding penetration of hemispherical-nosed rods.

2. Observation

In the present study, the ballistic threat consisted of a hemispherical-nosed, WA rod of the following characteristics: 65 g, length to diameter ratio (*L/D*) of 15, a content of 93% tungsten (W), 6.3% nickel (Ni) and 0.7% iron (Fe), and swaged (reduced in cross-sectional area) 8%. The W-Ni-Fe rods had a nominal hardness of R_C 37, with nominal dimensions of 101.9 mm long × 6.79 mm diameter. The target in these tests consisted of a stack of six 8 × 8 × 2.25 in

(nominal) Al-5083 blocks. The blocks were measured at a Brinell hardness of BHN 97 and a net target thickness of 344 mm.

The three experiments were conducted at impact velocities, V, of 1108, 1416, and 1701 m/s respectively. The two higher velocity (1416 and 1701 m/s) tests were above the erosion-threshold velocity and achieved penetrations, P, of 193.2 and 227.2 mm (Figure 1), respectively. These data are in agreement with the penetration model's prediction, if the rod's strength is characterized (with Tate-Alekseevskii parameters) at $Y = 1.1$ GPa, with the Al-5083 target resistance of $H = 1.78$ GPa. Such a characterization is wholly consistent with an R_C 37 WA penetrator and a BHN 97 Al target, ($\sigma_{ULT} = 0.31$ GPa), when one uses Tate's formulation for estimating H.

Were the remaining test, conducted at an impact velocity of 1108 m/s, to lie above the erosion-threshold velocity, one might have expected a penetration of ~164 mm into the Al-5083 target in question (Figure 1). However, this low-velocity test fell below the erosion-threshold velocity, and the rod in the experiment perforated the 344 mm target with a residual velocity, V_r, of 314 m/s. Additionally, a very fortunate circumstance arose in which the leading segment of the residual penetrator was recovered intact after the test. At first glance, the tip of the residual penetrator fragment, recovered after the test seemed to indicate that the rod had penetrated in a
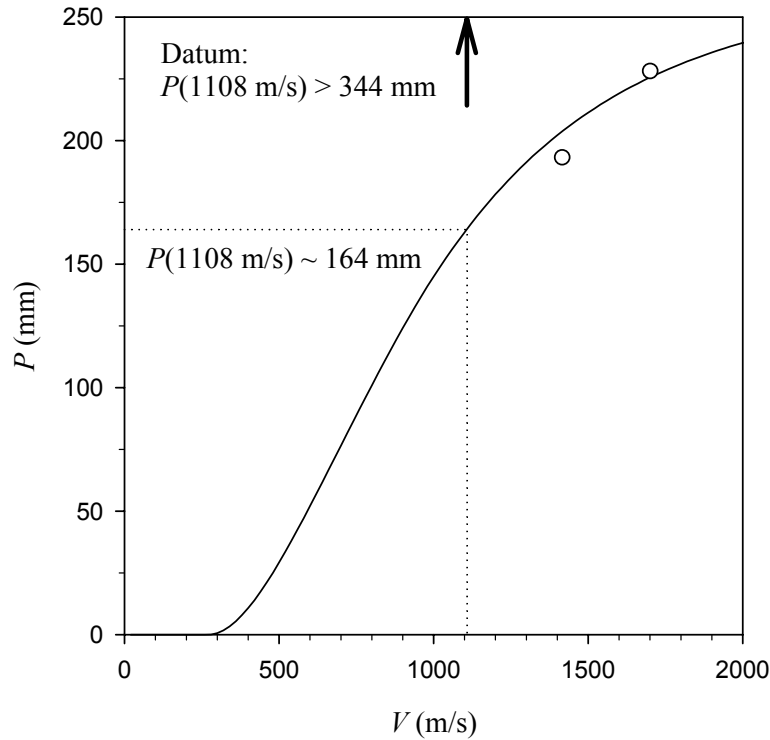

Figure 1. Model predictions and data for eroding WA rods into BHN 97 Al-5083 targets.

5

rigid-body fashion, as the hemispherical nose appeared intact and completely undeformed (Figure 2). Radiography behind the target captured two residual rod segments on film: the first, 61.5 mm long, which included the rod tip, and the second, 18.5 mm in length. There may have been additional rod segments to follow, accounting for the remaining 21.9 mm or original rod length; unfortunately, the exposure times of the radiographs would have placed them just inside the target and hence, not viewable. Note that the recovered fragment of Figure 2 is the leading part of the 61.5 mm segment, which subsequently fractured upon impact with the wall of the testing facility.
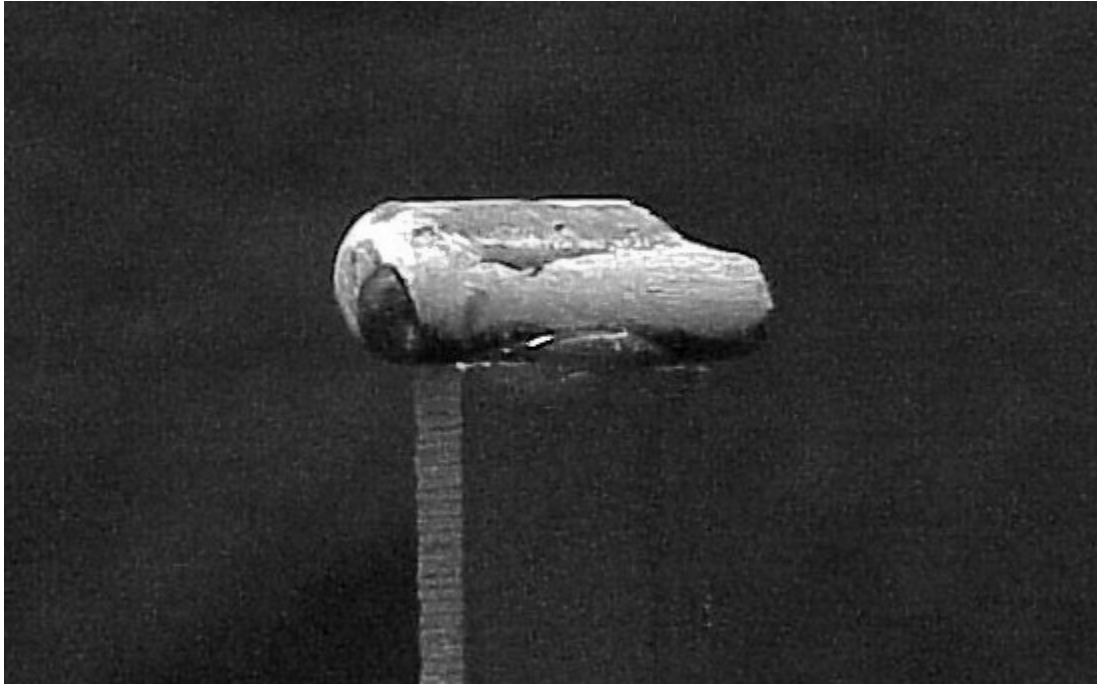
Figure 2. Residual rod-tip fragment recovered from noneroding test, with hemispherical nose intact.

Interestingly, a careful measurement of the post-mortem target crater and fortuitously recovered residual-rod fragment (Figure 3) from the low-velocity experiment revealed the following data: the rod diameter, as a result of the ballistic event, increased ~6% from 6.76 mm prior to the test to 7.19 mm; the crater diameter (except at the front entrance and accounting for yaw-induced crater ovalness) was ~6.40 mm. While there is some scatter in the crater diameter measurements, the final crater size was, nonetheless, observed to form an interference fit with not only the recovered residual fragment (7.19 mm), **but also an undeformed rod of identical nominal dimensions** (6.79 mm). While it is more complicated to estimate the actual rod and crater diameters during the course of the test, a co-equal value would have been necessary in order to permit the penetration to proceed. The fact that the postmortem rod/target diameter values differ is indicative of an elastic residual-stress relief (*i.e.*, crater-wall rebound) that has occurred following the passage of the rod. And while there is surely a finite time necessary for the crater wall to elastically rebound as the deformed rod's diameter varies along its length, it is

Figure 3. Crater cross-section of low-velocity test at a depth ~228 mm below the target surface
(residual rod fragment shown for scale).

highly plausible that, not only the tip, but much of the rear of the rod was also laterally engaged
with the target during the penetration event. Because of difficulty associated with edge detection
of radiographic images, it was impossible to estimate, from the exiting residual rod fragment
images, what length of the rod tip was bulged in diameter. And while the fracture and
subsequent separation of the two radiographed rod segments is indicative of a tensile fracture
61.5 mm from the rod tip, association of this dimension with rod bulging would be conjectural,
since both the rebound dynamics of the crater and the tensile reflections of the axial wave, off the
rear of the projectile, might both influence this event.

Comparable results to this in the literature, for hemispherical-nosed rods, would include those
reported by Scheffler (*21, 22*). Unfortunately, the only simulation detailed, in the case of the
deep penetration results (*21*), was at an impact velocity above the erosion threshold
(1296 m/s), and so the computationally predicted rod deformation was significantly more
extensive than observed presently at 1108 m/s. In the case of finite target perforations (*22*), there
is a datum at 1147 m/s for the case of a hemispherical-nosed rod against a 76.2 mm thick
Al-5083 target. In addition to the vast difference in target thickness (76.2 mm vs. 344 mm
presently), the rods reported on by Scheffler (*22*) were 95% W, compared to the 93% rods tested
for this report. The depiction of the radiographically imaged residual penetrator is too small and
coarse to detect deformations near the rod tip, and Scheffler characterizes the experiment as
"rigid." It is difficult to discern whether his corresponding CTH simulations show a visible
flattening of the rod tip, because of the limited simulation resolution and the presence of Eulerian

mixed-cells. The simulations do, however, show an equivalent plastic strain between 5% and 12% in the leading one to three rod diameters of rod length (the plastic extent depending upon the simulation mixed-cell methodology). Such an observation of strain is compatible with the presently recovered fragment of Figure 2, which exceeds two rod diameters in length, with a radial strain of 6% (plastic incompressibility would imply an axial strain, here, of -12%).

The photographs in the work of Forrestal and Piekutowski (*24*) also corroborate the present observation of a noticeably expanded, but noneroded tip diameter, at velocities below the erosion threshold. While they don't explicitly report the diameter expansion of the noneroded rods, they do report the associated length compaction, which in one case resulted in a 10.2 mm length shrinkage on a 71.1 mm rod. Such strains are on a comparable scale to the diameter expansions presently observed.

The most detailed description of the plastic-yet-noneroding phenomenology is the aforementioned extended quotation by Magness and Scheffler (*23*). However, that description is specifically for the case of an ogival-nosed penetrator. Nonetheless, it would appear, on the basis of the postmortem data from the present experiment, that the noneroding phenomenology described by Magness and Scheffler (*23*) for ogival penetrators applies identically to that for hemispherical-nosed penetrators. This result is striking, given that Magness and Scheffler astutely observed that, above the erosion-threshold velocity, ogival-nosed penetration phenomenology most closely follows that of conical-nosed penetrators (*23*), rather than hemispherical-nosed penetrators.

Finally, despite the similarity of penetration phenomenology for noneroding hemispherical- and ogival-nosed penetrators, the erosion-threshold velocities for penetrators with these two nose shapes is significantly different (*21, 22*), but understandably so. Hill (*10*) recognized early that the propensity for cavitation was intimately related to the local radius of curvature of the rod nose. The geometrical profiles, and thus the radii of curvature and, by deduction, the propensity for cavitation (thus, erosion) will be different for hemispherical- and ogival-nosed penetrators.

3. Analysis

While the cited works reveal a thoughtful consideration of the low-velocity penetration phenomenon, there are still gaps in the understanding of this process, most particularly with regard to the analytical modeling of the penetration process below the erosion-threshold velocity, when plasticity is nonetheless involved. Much detailed and thorough analysis has been offered in the literature by Hill (*10*) and Forrestal *et al.* (*12–16*), but in these cases the analyses limit the engagement conditions so as to preclude the possibility of rod plasticity, *a priori*. So while they provide much to draw upon when considering rigid-body penetration, they do not answer all the questions associated with plastic, yet noneroding, penetration.

Yatteau and Dzwilewski (*20*) presented an initial outline for an analytical model for the penetration of conical-nosed penetration. For the limited condition in which plasticity occurs, yet prior to rod erosion, the criterion they use to establish this condition is whether the rod's foreshortening rate, *V–U*, is less than the rod's plastic wave speed. If so, the plasticity associated with the rod foreshortening is assumed to be "accommodated" by radial expansion at the tip and "presumed to become part of the rigid nose piece." While they are correct in asserting that a foreshortening rate above the plastic wave speed cannot be accommodated by plasticity at the nose of the rod, there is no guarantee, on the other hand, that a foreshortening rate below the plastic wave speed *must* be accommodated by plasticity at the nose, especially as *V–U* approaches the plastic wave speed.

One interesting aspect that has not been addressed adequately in the literature is the inability of traditional penetration methodology (*e.g.*, Tate/Alekseevskii methodology [*2, 3*]) to account for the observed discontinuity of penetration behavior across the erosion-transition barrier. The kinematic statements of rod erosion and penetration (*P*) are, respectively,

$$\dot{L} = \dot{U} - \dot{V} \quad ; \tag{1}$$

$$\dot{P} = U \quad , \tag{2}$$

where *L* is rod length and the dot indicates time differentiation. Rod deceleration is obtained by way of force/momentum balance on the elastic portion of the rod,

$$L\dot{V} = -Y / \rho_R \quad . \tag{3}$$

The other vital component to traditional penetration methodology is the force/momentum balance in the rod/target stagnation zone,

$$k_R \rho_R (V - U)^2 + Y = k_T \rho_T U^2 + H \quad . \tag{4}$$

This latter equation indicates that the stress at the rod/target interface, balanced on both the rod and target sides, is composed of an axial strength term superimposed over the stagnation stress of the flow field along the centerline. In the traditional penetration methodology (*2, 3*), the parameters k_R, Y, k_T, and H are considered constants.

The parameters k_R and k_T are so-called "shape factors" for the rod and target respectively, associated with the manner in which the rod/target stagnation flow is split. With a blunt-nosed rod or an eroding interface that naturally establishes a blunt profile, these parameters take on the value of 1/2, in accordance with the dictates of Bernoulli stagnation flow. For geometries where the stagnation flow experiences a turning angle other than 90°, Segletes *et al.* (*7*) noted that the functionality of this variation in *k* should proceed as 1/2 (1−cosδ), where δ is the angle of flow turning. In the case, for example, of rigid penetration by a conical-nosed rod, the angle δ

corresponds to the half angle of the nose of the rod, in the calculation of k_T (note that k_R becomes irrelevant as V–U becomes zero for rigid penetration). The parameter Y is a strength term that characterizes the rod, and is typically associated with the uniaxial compressive strength of the rod. On the other hand, H is the target resistance, a strength term associated with resistance to penetration. While related to the compressive strength of the target, the value of H is, for a ductile target, typically 3 to 5 times the uniaxial compressive strength of the target material, compatible with various theories of indentation and crater formation.

Employing this theory with fixed parameters k_R, Y, k_T, and H reveals the following: the penetration vs. velocity curves arising from the traditional methodology, such as that in Figure 1, will always produce a smooth curve with no abrupt renormalization as rigid-body penetration transitions to an eroding-rod configuration.

Rather, in order to capture the sudden penetration dislocation associated with the erosion transition, as a minimum, one or more of the traditional, fixed parameters k_R, Y, k_T, and H needs to be varied as a function of the penetration mode. For the rigid penetration of conical-nosed rods, it has already been described how the k_T parameter is dependent upon the cone angle of the nose. Such a variation can account for the penetration disparity of various conical-nosed rods of differing nose angles. Furthermore, were the nose to be blunted following the transition to eroding penetration, the value of k_T could arguably revert back to the 1/2 value. Nonetheless, the penetration methodology for conical-nosed rods depicted by Woodward (*17, 18*) would not seem to indicate a sudden reversion to blunt-nosed erosive penetration, at velocities immediately above the erosion-transition velocity.

While the penetration-mode dependence of k_T and k_R might be reasonably argued for conical or other sharp-nosed penetrators (including ogival-nosed rods), it is much harder to justify for ductile hemispherical-nosed rods, since the shape of the target's (hemispherical) flow field is self-similar in both noneroding and eroding modes. Such is the case for the current analysis, involving hemispherical-nosed W rods impacting Al-5083 targets. This would leave as the only option, in an attempt to model the erosion-threshold transition, the penetration-mode variation of rod strength and target resistance parameters, Y and H, respectively.

Frank (*26*) modeled the penetration behavior across the erosion threshold in the mid 1990s by decreasing the target's surface resistance vis-à-vis the core resistance, H. In this report, however, we instead choose to examine and model the noneroding-penetration problem by examining the influence of penetration mode upon the "rod strength" parameter, Y. Consider the ballistic-stress balance of equation 4 for the case of noneroding penetration, in which $U = V$:

$$Y = \frac{1}{2}\rho_T V^2 + H \quad . \tag{5}$$

In the case of the noneroding impact presently observed at 1108 m/s, the target's inertial head alone, equal to $1/2\rho_T V^2$, computes to 1.66 GPa, far in excess of the 1.1 GPa rod strength associated with an R_C 37 tungsten penetrator. The $H = 1.78$ GPa target resistance coupled with this inertial head would require a rod strength of $Y \geq 3.44$ GPa in order to retain rigidity. Ballistic rod strength of 3.44 GPa is more than triple the 1.1 GPa amount estimated for the rod on the basis of both the W's intrinsic properties as well as the two other similar ballistic tests. Such a disparity between actual and apparent rod strength leaves the one-dimensional traditional analytical modeling wanting for a credible explanation.

That the recovered rod fragment of Figure 2 indicates noneroding penetration leads to the probing question: if the rod were, in some way, able to feign strength in excess of 3.44 GPa, would the analytical model prediction for the penetration of a rod, with this fictitious strength, match the noneroding penetration datum? While an affirmative reply to this query would not reveal how the feat was accomplished, it would nonetheless indicate that the solution to analytically addressing the problem is properly accomplished through an increase in apparent rod strength, rather than a decrease in the target resistance. It would also indicate that the rod, for all practical purposes, did penetrate *as if* it were a rigid body and *as if* it had a yield strength in excess of 3.44 GPa. Figure 4 presents the results of the model and data, which strikingly shows the validity of this conjecture. But while one may conclude that the noneroding rod penetrated as if it were a rigid penetrator with strength three times its nominal value, the question remains as to the proper manner and interpretation by which this phenomenon may be incorporated into the framework of analytical modeling.

4. Interpretation

The cratering phenomenology for noneroding penetration is notably different from that arising as a result of eroding penetration. Above the erosion threshold, the crater profile is rough and somewhat larger than the rod diameter (more than 1.5× in the current testing). By contrast, the crater profile for noneroding penetration is smooth and appears to remain at a size approximately equal to the rod-diameter. Indeed, for the noneroding impact observed at 1108 m/s, the crater diameter was actually slightly smaller than that of the rod, indicating an interference fit during the penetration event.

This disparity in the crater formation between the eroding and noneroding penetration leads to the inference that the reason that the plastic, yet noneroding, rod fails to erode was because the penetration cavity being formed was too small to permit rod material to turn away from the rod trajectory, so as to deposit itself (in the traditional sense of an eroding rod penetrator) on the crater wall. Wijk (*11*) seems cognizant of this condition wherein the rod is unable to flow radially in the eroding-rod sense. He goes so far as to calculate both the minimum crater radius needed to permit an eroding-flow field, as well as the corresponding penetration velocity needed
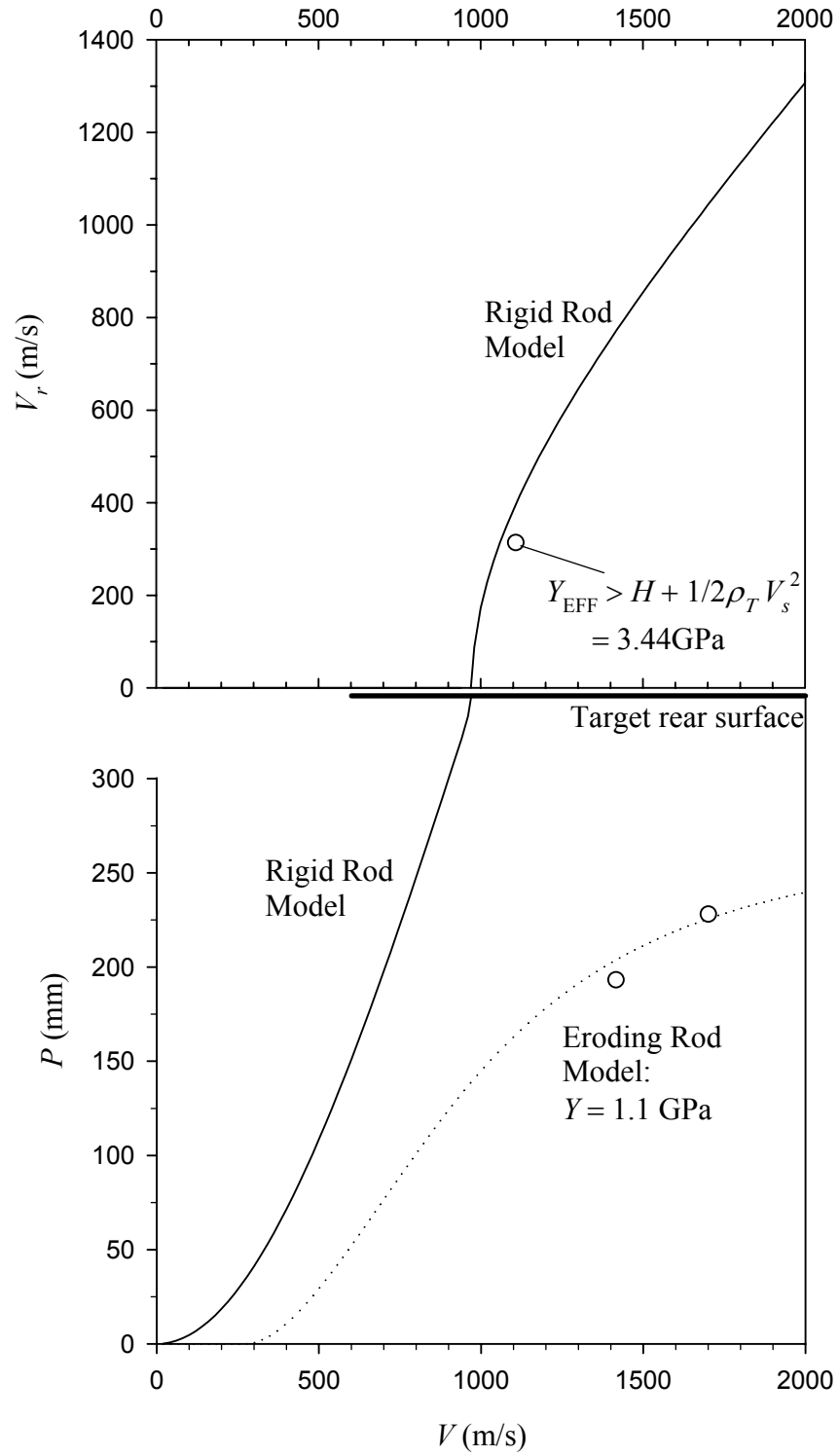
Figure 4. Model predictions and data of penetration and residual-velocity, for (rigid and $Y = 1.1$ GPa) WA rods into 344 mm thick BHN 97 Al-5083 target (target rear surface modeled with plastic-zone extent: 3.5; spall resistance: $H_{SPALL} = H/3$ [1, 7]).

12

to achieve this crater radius. Wijk's primary intent seems to be on the end stage of penetration, wherein the penetration velocity of an eroding rod decreases to the point where traditional eroding penetration is no longer possible, resulting in an alternate phenomenology of penetration.

Using Wijk's equations with the current material properties (ρ_T = 2700 kg/m³, Y_T = 0.31 GPa, target shear modulus G_T = 30 GPa, ρ_R = 17600 kg/m³, Y_R = 1.1 GPa) yields an estimation of erosion-threshold velocity at 866 m/s. The present data show the erosion-threshold velocity to be between 1100 and 1400 m/s. Scheffler's analyses (21, 22) further constrain this value below 1200 m/s and indicate a rod-nose-shape dependence to even this result.

Wijk, despite the quantitative discrepancy, deserves credit for understanding certain facets of what defines this erosion-threshold velocity, wherein the crater is large enough a diameter to permit the establishment of an eroding flow field in the rod. However, it does not appear that his comprehension of the altered penetration phenomenology resulting from it extended to the present form of noneroding behavior, as he explicitly states that "for maximum penetration capacity the rear part of the projectile must be able to pass the lined hole created by the front part" (11). The present datum belies this assumption. And while, as a point of reference, the noneroding datum achieved a P/L = 3.37 with significant residual velocity (V_r/V = 0.28), Wijk dismissed the possibility that a rod would achieve even hydrodynamic levels of penetration (P/L = 2.55 for tungsten on aluminum) at low-impact velocities as "of course an unrealistic result" (11).

Having inferred that the rod is unable to erode because the radial flow is constrained does not directly answer the question, however, of how a 1.1 GPa rod is able to remain noneroding while exerting the necessary 3.44 GPa of stress at the penetrator/target interface. For more quantitative insight, consider also prior qualitative explanations of the process. Brooks and Erikson's (9) characterization of the rod's ogival nose being "supported hydrostatically by the target material," and Magness and Scheffler's (23) contention that the ogival nose of the rod is eventually "constrained by the surrounding armor material and loaded under triaxial compression" are both directly supportive of the notion that the rod material is attempting to turn away from the rod's axial trajectory, but is unable to do so fully, for lack of radial inertia.

The idea that the "hydrostatic" or "triaxial" stress might play a key role for hemispherical-nosed rods, as well, is completely corroborated by the interference fit observed between the residual rod and the target crater that resulted from the 1108 m/s impact in the current test series. While it may not be readily apparent how this realization should be represented in the Bernoulli stress balance of equation 4, one may draw upon Segletes and Walters (27), who rederived various interpretations of the penetration equations through a derivation and application of a highly generalized "extended" Bernoulli equation.

The characterization of the stress that manifests itself as Y in equation 4 is predicated upon the assumed uniaxial stress field within the elastic portion of the rod. The actual term, as indicated in the generalized derivation of Segletes and Walters (25), is really σ_{zz} and not Y (σ_{zz} being the

13

normal stress in the coordinate direction of penetration). In the presumed absence of a laterally induced stress component (and consistent with Tate's original derivation), the axial stress magnitude of σ_{zz} in the noneroding rod is thus limited by the rod strength, Y. In the presence, however, of a lateral stress component σ_{LAT}, induced in the rod by the lateral interference with the target, the generalized axial rod-stress term, σ_{zz}, will manifest itself as $Y + \sigma_{LAT}$, in accordance with Tresca yielding. This revision will yield a ballistic-stress balance of

$$\frac{1}{2}\rho_R(V-U)^2 + (Y + \sigma_{LAT}) = \frac{1}{2}\rho_T U^2 + H \quad , \tag{6}$$

where σ_{LAT} is positive in compression. When, as in the current case, the lateral stress provokes noneroding penetration (wherein $U = V$), the magnitude of the stress may be explicitly calculated as

$$\sigma_{LAT} = \frac{1}{2}\rho_T V^2 + H - Y \quad . \tag{7}$$

That the hemispherical cap of the deformed (postmortem) rod remained intact indicates the absence of erosive flow during the penetration event and leads one to a particular kinematic interpretation, consistent with the qualitative description of Magness and Scheffler (*23*), given for ogival rods. Namely, during the initial stages of penetration, the rod's inertia, under force of impact, causes the rod to compress axially and expand radially in a plastic manner. Such behavior is not unlike the early stages of a Taylor impact test, excepting the fact that the rod is simultaneously embedding itself into the target material. The rod (or the leading portion thereof) expands radially in full contact with and against the target, in a controlled manner, until such time that sufficient radial expansion has been imposed upon the target to raise the lateral-interface stress to a level of 2.34 GPa, acting as a confining stress σ_{LAT} upon the rod. At this time, the rod's axial stress, being composed of $Y + \sigma_{LAT}$, is brought the level of 3.44 GPa, sufficient to trigger rigid-body penetration in the target, and arrest further plastic, axial compression of the rod.

Unlike traditional penetration theory, wherein the rod (excepting the tip) penetrates in a state of presumed uniaxial stress, the leading portion of the rod in the noneroding case penetrates under the condition of triaxial rod stress ($\sigma_{zz} = 3.44$ GPa, $\sigma_{xx} = \sigma_{yy} = 2.34$ GPa in this case). This interference fit of the rod and target crater becomes the necessary facilitator for the elevated penetration behavior, for it allows the axial stress brought to bear, by the rod upon the target, to be composed of a uniaxial strength component (traditionally associated with Y) augmented by a superimposed pressure component (transmitted laterally from the target). In so doing, it allows the utilization of the target's lateral resistance to great axial effect.

At higher velocities, Wijk's (*11*) explanation holds true qualitatively, if not quantitatively. Namely, at a large enough velocity, the radial expansion of the forming crater becomes large

enough to permit room for flow turning in the rod, thereby kinematically allowing for erosive flow of the penetrator. Once this flow turning occurs, the rod's tip is robbed of its laterally induced triaxial-stress support. In that event, the stress across the rod/target interface must instead be balanced by way of added inertial stress, generated from the stagnation of the eroding-rod flow. According to the present data, this threshold velocity would fall between 1108 and 1416 m/s. Scheffler's computations (*21*) would further indicate the erosion threshold to fall below 1200 m/s for hemispherical-nosed W rods onto Al-5083, but with a strong nose-shape dependence on this threshold.

It would seem that the nose-shape dependence of the transition velocity, while not addressed here, is related more to the local curvature of the nose geometry. An approach that incorporates the reasoning of Hill (*10*) or Forrestal *et al.* (*12*), in this regard, might provide the necessary insight to adequately predict the effect of nose geometry on threshold velocity.

5.   Conclusions

This report analyzes ballistic data for WA rods penetrating Al-5083 targets in the vicinity of the erosion-threshold velocity. Attention was directed at the one-dimensional modeling of the noneroding penetration event. Conventional one-dimensional penetration analysis reveals that the penetration and residual velocity in this test was wholly consistent with the notion of treating the rod *as if* it penetrated in a rigid-body fashion, and possessing an unrealistically large yield strength in excess of 3.4 GPa. Such strength is more than triple the 1.1 GPa value inferred from hardness measurements and other ballistic testing.

Study of a recovered postmortem rod fragment and the target from the noneroding test revealed that, in fact, the penetrating rod deformed plastically, but did so without erosion. The evidence of rod plasticity was a ~6% increase in rod diameter between the original rod and the recovered postmortem rod fragment. Supported by analysis is the hypothesis that the rod did, in fact, apply a 3.44 GPa axial stress to the target interface. However, that stress comprised both the rod's intrinsic 1.1 GPa yield strength plus a 2.34 GPa confining stress caused by a lateral interference fit between the rod and target crater during the penetration event. In such a fashion, the rod was able to employ the target's lateral strength to great axial advantage. Higher velocity tests did not exhibit the noneroding behavior, precisely because the higher impact velocities created large enough craters in the target to remove the lateral interference that had augmented the axial stress at lower velocities. In so doing, the flow field in the rod was permitted to turn, creating the necessary conditions, according to Wijk (*11*), to establish an eroding flow field.

The literature concerning the penetration of rods with different nose shapes (*e.g.*, conical, ogival, hemispherical) has shown unique phenomenologies near the erosion threshold. Above the rod-erosion threshold, Magness and Scheffler noted that ogival-nosed rods exhibit a morphology

similar to conical-nosed rods (*9*, *17*) in establishing a rigid embedded tip ahead of an eroding rod shank. Scheffler's earlier results (*21*, *22*) would indicate that eroding hemispherical rods do not establish this embedded tip. The current work buttresses this literature by helping to establish that, below the rod-erosion threshold, the behavior of hemispherical-nosed rods is characteristically similar to that of ogival-nosed rods, whose penetration phenomenology was clearly laid out by Magness and Scheffler (*23*).

Thus, it would seem that smooth transition from rod tip to shank (*i.e.*, when the slope of the rod's geometric profile is continuous), evident in both ogival- and hemispherical-nosed rods helps to retard cavitation (*i.e.*, retards the separation of target from rod). In so doing, it establishes the capacity for rods of these nose profiles to utilize plastic, yet noneroding, penetration to a greater extent than their conical-nosed counterparts. In contrast, above the erosion threshold, the sharp point of both ogival- and conical-nosed rods produces a stress field that resists an erosive flattening of the rod nose. In so doing, there is a propensity for rods of these nose profiles to establish a pointed, rigid, embedded tip ahead of an eroding rod shank, not evident in ductile hemispherical-nosed rods.

6. References

1. Segletes, S. B. *An Adaptation of Walker-Anderson Model Elements Into the Frank-Zook Penetration Model for Use in MUVES*; ARL-TR-2336; U.S. Army Research Laboratory: Aberdeen Proving Ground, MD, 2000.

2. Tate, A. A Theory for the Deceleration of Long Rods After Impact. *Journal of Mechanics and Physics of Solids* **1967**, *15*, 387–399.

3. Alekseevskii, V. Penetration of a Rod Into a Target at High Velocity. *Combustion, Explosions and Shock Waves* **1966**, *2*, 63–66.

4. Zook, J. A.; Frank, K.; Silsby, G. F. *Terminal Ballistics Test and Analysis Guidelines for the Penetration Mechanics Branch*; BRL-MR-3960; U.S. Army Ballistic Research Laboratory: Aberdeen Proving Ground, MD, 1992.

5. Wright, T. W.; Frank, K. *Approaches to Penetration Problems*; BRL-TR-2957; U.S. Army Ballistic Research Laboratory: Aberdeen Proving Ground, MD, 1988.

6. Walker, J. D.; Anderson, C. E. Jr. A Time-Dependent Model for Long-Rod Penetration. *International Journal of Impact Engineering* **1995**, *16* (1), 19–48.

7. Segletes, S. B.; Grote, R.; Polesne, J. *Improving the Rod-Penetration Algorithm for Tomorrow's Armors*; ARL-RP-23; U.S. Army Research Laboratory: Aberdeen Proving Ground, MD, 2001.

8. Kinslow, R. Collisions at High Velocity. *International Science and Technology* **1965**, *40*.

9. Brooks, P. N.; Erikson, W. H. *Ballistic Evaluation of Materials for Armour Penetrators*; DREV R-643/71; Defence Research Establishment Valcartier, Quebec, Canada, 1971.

10. Hill, R. Cavitation and the Influence of Headshape in Attack of Thick Targets by Non-Deforming Projectiles. *Journal of Mechanics and Physics of Solids* **1980**, *28*, 249–263.

11. Wijk, A. G. High-Velocity Projectile Penetration Into Thick Armour Targets. *International Journal of Impact Engineering* **1999**, *22*, 45–54.

12. Forrestal, M. J.; Okajima, K.; Luk, V. K. Penetration of 6061-T651 Aluminum Targets With Rigid Long Rods. *Journal of Applied Mechanics* **1988**, *55*, 755–760.

13. Rosenberg, A.; Forrestal, M. J. Perforation of Aluminum Plates With Conical-Nosed Rods – Additional Data and Discussion. *Transactions of the ASME* **1988**, *55*, 236–238.

14. Forrestal, M.; Luk, V. K. Perforation of Aluminum Armor Plates With Rigid Conical-Nose Projectiles. *Mechanics of Materials* **1990**, *10*, 97–105.

15. Forrestal, M.; Brar N. S.; Luk, V. K. Penetration of Strain-Hardening Targets With Rigid Spherical-Nose Rods. *Journal of Applied Mechanics* **1991**, *58*, 7–10.

16. Forrestal, M.; Luk, V. K.; Rosenberg, Z.; Brar N. S. Penetration of 7075-T651 Aluminum Targets with Ogival-Nose Rods. *International Journal of Solids and Structures* **1992**, *29* (14/15), 1729–1736.

17. Woodward, R. L. A Note on the Deformation of Conical Penetrators. *International Journal of Impact Engineering* **1984**, *2* (4), 325–330.

18. Woodward, R. L. The Effect of Projectile Tip Geometry on Penetration Into Semi-Infinite Metal Targets. *Proceedings of 9th International Symposium on Ballistics*, Shrivenham, U.K., May, 1986.

19. Chen, E. P. Finite Element Simulation of Perforation and Penetration of Aluminum Targets by Conical-Nosed Steel Rods. *Mechanics of Materials* **1990**, *10,* 107–115.

20. Yatteau, J. D.; Dzwilewski, P. T. The Onset of Deformation and Flow in Penetrators With Conical Noses. *Proceedings of 15th International Symposium on Ballistics*, Jerusalem, Israel, 21–24 May 1995.

21. Scheffler, D. R. *Modeling the Effect of Penetrator Nose Shape on Threshold Velocity for Thick Aluminum Targets*; ARL-TR-1417; U.S. Army Research Laboratory: Aberdeen Proving Ground, MD, 1997.

22. Scheffler, D. R. *Modeling Threshold Velocity of Hemispherical and Ogival-Nose Tungsten-Alloy Penetrators Perforating Finite Aluminum Targets*; ARL-TR-1583; U.S. Army Research Laboratory Report: Aberdeen Proving Ground, MD, 1998.

23. Magness, L. S.; Scheffler, D. R. The Influence of Penetrator Material and Projectile Nose Shape on the Onset of Penetrator Deformation and Erosion. *Proceedings of 2nd Australasian Conference on Applied Mechanics*, Canberra, Australia, February 1999.

24. Forrestal, M. J.; Piekutowski, A. J. Penetration Experiments With 6061-T6511 Aluminum Targets and Spherical-Nose Steel Projectiles at Striking Velocities Between 0.5 and 3.0 km/s.” *International Journal of Impact Engineering* **2000**, *24*, 51–67.

25. Piekutowski, A. J.; Forrestal, M. J.; Poorman, K. L.; Warren, T. L. Penetration of 6061-T6511 Aluminum Targets by Ogive-Nose Steel Projectiles With Striking Velocities Between 0.5 and 3.0 km/s. *International Journal of Impact Engineering* **1999**, 23, 723–734.

26. Frank, K. U.S. Army Research Laboratory: Aberdeen Proving Ground, MD. Private communication, citing unpublished results, 2003.

27. Segletes, S. B.; Walters. W. P. A Note on the Application of the Extended Bernoulli
    Equation. *International Journal of Impact Engineering* **2002**, *27*, 561–576.

20

5   DEFENSE NUCLEAR AGENCY
MAJ J LYON
CDR K W HUNTER
T FREDERICKSON
R J LAWRENCE
SPSP K KIBONG
6801 TELEGRAPH RD
ALEXANDRIA VA 22310-3398

2   COMMANDER
US ARMY ARDEC
AMSTA AR FSA E
W P DUNN
E BAKER
PICATINNY ARSENAL NJ
07806-5000

1   COMMANDER
US ARMY ARDEC
AMSTA AR CCH V M
D NICOLICH
PICATINNY ARSENAL NJ
07806-5000

1   COMMANDER
US ARMY ARDEC
E ANDRICOPOULOS
PICATINNY ARSENAL NJ
07806-5000

1   COMMANDER
USA STRATEGIC DEFNS CMD
CSSD H LL
T CROWLES
HUNTSVILLE AL 35807-3801

4   COMMANDER
US ARMY AVIATION & MISSLE CMD
AMSAM RD PS WF
S HILL
D LOVELACE
M SCHEXNAYDER
G SNYDER
REDSTONE ARSENAL AL 35898-5247

1   COMMANDER
US ARMY AVIATION & MISSLE CMD
AMSAM RD SS AA
J BILLINGSLEY
REDSTONE ARSENAL AL 35898

1   MIS DEFNS & SPACE TECHNOLOGY
CSSD SD T K H JORDAN
PO BOX 1500
HUNTSVILLE AL 34807-3801

3   COMMANDER
US ARMY RESEARCH OFFICE
K IYER
J BAILEY
S F DAVIS
PO BOX 12211
RESEARCH TRIANGLE PARK NC
27709-2211

1   NAVAL AIR WARFARE CTR
S A FINNEGAN
BOX 1018
RIDGECREST CA 93556

4   COMMANDER
NAVAL WEAPONS CENTER
N FASIG
CODE 3261
T T YEE
CODE 3263
D THOMPSON
CODE 3268
W J MCCARTER
CODE 6214
CHINA LAKE CA 93555

12   COMMANDER
NAVAL SURFACE WARFARE CTR
DAHLGREN DIVISION
H CHEN
D L DICKINSON CODE G24
C R ELLINGTON
C R GARRETT CODE G22
W HOLT CODE G22
W E HOYE G22
R MCKEOWN
JOHN M NELSON
M J SILL CODE H11
WILLIAM J STROTHER
A B WARDLAW JR
L F WILLIAMS CODE G33
17320 DAHLGREN RD
DAHLGREN VA 22448

2   AIR FORCE ARMAMENT LAB
AFATL DLJR
J FOSTER
D LAMBERT
EGLIN AFB FL 32542-6810

NO. OF COPIES	ORGANIZATION	NO. OF COPIES	ORGANIZATION
1	USAF PHILLIPS LABORATORY VTSI ROBERT ROYBAL KIRTLAND AFB NM 87117-7345		<u>SANDIA NATIONAL LAB CONT'D</u> MS0819 P TAYLOR R BRANNON
2	USAF PHILLIPS LABORATORY PL WSCD F ALLAHDADI PV VTA D SPENCER 3550 ABERDEEN AVE SE KIRTLAND AFB NM 87117-5776		MS0820 M KIPP MS0820 D CRAWFORD MS0820 L CHHABILDAS
1	AFIT ENC D A FULK WRIGHT PATTERSON AFB OH 45433		MS0821 P STANTON MS0821 J M MCGLAUN
1	MICHAEL G LEONE FBI FBI LAB EXPLOSIVES UNIT 935 PENNSYLVANIA AVE NW WASHINGTON DC 20535		MS0835 E S HERTEL JR MS0836 L N KMETYK MS0980 R REEDER
7	LOS ALAMOS NATIONAL LAB L HULL MS A133 J V REPA MS A133 J WALTER MS C305 C WINGATE MS D413 E J CHAPYAK MS F664 P HOWE MS P915 J KENNEDY MS P915 PO BOX 1663 LOS ALAMOS NM 87545		MS0980 J SOUTHWARD MS0980 R LAFARGE MS0986 R TACHAU MS1156 M FURNISH MS1168 M FORRESTAL MS1174 W REINHART MS1181 D HAYES MS1181 J ASAY MS1181 E W REECE
31	SANDIA NATIONAL LAB ATTN MAIL SERVICES MS 0100 J ANG MS0310 P YARRINGTON MS0310 W TEDESCHI MS0479 B LEVIN MS0706 A ROBINSON MS0819 T TRUCANO MS0820		MS1185 D P KELLY MS1185 C HALL MS1209 J COREY MS1217 C HILLS MS1411 M VIGIL MS1454 R O NELLUMS PO BOX 5800 ALBUQUERQUE NM 87185-0100

NO. OF COPIES	ORGANIZATION	NO. OF COPIES	ORGANIZATION
3	DIR LLNL MS L35 D BAUM M MURPHY T MCABEE PO BOX 808 LIVERMORE CA 94550	2	DIR LLNL MS L180 G SIMONSON A SPERO PO BOX 808 LIVERMORE CA 94550
7	DIR LLNL MS L122 R PIERCE R ROSINKY O J ALFORD D STEWART T VIDLAK B R BOWMAN W DIXON PO BOX 808 LIVERMORE CA 94550	1	DIR LLNL F A HANDLER L182 PO BOX 808 LIVERMORE CA 94550
		1	DIR LLNL MS L282 W TAO PO BOX 808 LIVERMORE CA 94550
2	DIR LLNL MS L125 D R FAUX N W KLINO PO BOX 808 LIVERMORE CA 94550	2	DIR LLNL MS L290 A HOLT J E REAUGH PO BOX 808 LIVERMORE CA 94550
1	DIR LLNL MS L149 R VAROSH PO BOX 808 LIVERMORE CA 94550	1	DIR LLNL S G COCHRAN L389 PO BOX 808 LIVERMORE CA 94550
1	DIR LLNL R BARKER L159 PO BOX 808 LIVERMORE CA 94550	2	DIR LLNL MS L495 D GAVEL J HUNTER PO BOX 808 LIVERMORE CA 94550
3	DIR LLNL MS L163 M FINGER R PERRET W SHOTTS PO BOX 808 LIVERMORE CA 94550	1	DIR LLNL R M KUKLO L874 PO BOX 808 LIVERMORE CA 94550
3	DIR LLNL MS L178 H KRUGER G POMYKAL M GERASSIMENKO PO BOX 808 LIVERMORE CA 94550	4	ENERGETIC MATERIALS RSCH TESTNG CTR NEW MEXICO TECH D J CHAVEZ L LIBERSKY F SANDSTROM M STANLEY CAMPUS STATION SOCORRO NM 87801

NO. OF COPIES	ORGANIZATION
3	NASA JOHNSON SPACE CENTER E CHRISTIANSEN J L CREWS F HORZ MAIL CODE SN3 2101 NASA RD 1 HOUSTON TX 77058
1	APPLIED RESEARCH LAB J A COOK 10000 BURNETT ROAD AUSTIN TX 78758
4	JET PROPULSION LABORATORY IMPACT PHYSICS GROUP Z SEKANINA P WEISSMAN B WEST J ZWISSLER 4800 OAK GROVE DR PASADENA CA 91109
2	BROWN UNIVERSITY R CLIFTON ENGNG P SCHULTZ GEO SCI PROVIDENCE RI 02912
2	CAL TECH J SHEPHERD MS 105 50 A P INGERSOLL MS 170 25 1201 E CALIFORNIA BLVD PASADENA CA 91125
1	CAL TECH G ORTON MS 169 237 4800 OAK GROVE DR PASADENA CA 91007
2	DREXEL UNIVERSITY MEM DEPT A ZAVALIANGOS DEPT MAT ENGNG 32ND & CHESTNUT ST PHILADELPHIA PA 19104
1	GEORGIA INSTITUTE OF TECHNOLOGY COMPUTATIONAL MODELING CTR S ATLURI ATLANTA GA 30332-0356

NO. OF COPIES	ORGANIZATION
1	GEORGIA INSTITUTE OF TECHNOLOGY SCHOOL OF MATH SCIENCE & ENGNG K LOGAN ATLANTA GA 30332-0245
1	JOHNS HOPKINS UNIVERSITY MAT SCI & ENGNG DEPT M LI 102 MARYLAND HALL 3400 N CHARLES ST BALTIMORE MD 21218-2689
5	JOHNS HOPKINS UNIVERSITY APPLIED PHYSICS LAB T R BETZER A R EATON R H KEITH D K PACE R L WEST JOHNS HOPKINS ROAD LAUREL MD 20723
1	LOUISIANA STATE UNIVERSITY R W COURTER 948 WYLIE DR BATON ROUGE LA 70808
1	NC STATE UNIVERSITY Y HORIE RALEIGH NC 27695-7908
1	PENNSYLVANIA STATE UNIVERSITY PHYSICS DEPT UNIVERSITY PARK PA 16802
4	SOUTHWEST RESEARCH INSTITUTE C ANDERSON S A MULLIN J RIEGEL J WALKER PO DRAWER 28510 SAN ANTONIO TX 78228-0510
1	SUNY STONEYBROOK DEPT APPL MATH & STAT J GLIMM STONEYBROOK NY 11794

NO. OF COPIES	ORGANIZATION	NO. OF COPIES	ORGANIZATION
1	UC BERKELEY MECHANICAL ENGINEERING DEPT GRADUATE OFFICE K LI BERKELEY CA 94720	1	VIRGINIA POLYTECHNIC INSTITUTE COLLEGE OF ENGRNG DEPT ENGNG SCIENCE & MECHANICS R C BATRA BLACKSBURG VA 24061-0219
2	UC SAN DIEGO DEPT APPL MECH & ENGR SVCS R011 S NEMAT NASSER M MEYERS LA JOLLA CA 92093-0411	2	AEROJET J CARLEONE S KEY PO BOX 13222 SACRAMENTO CA 95813-6000
2	UNIV OF ALA HUNTSVILLE AEROPHYSICS RSCH CTR G HOUGH D J LIQUORNIK PO BOX 999 HUNTSVILLE AL 35899	2	AEROJET ORDNANCE P WOLF G PADGETT 1100 BULLOCH BLVD SOCORRO NM 87801
1	UNIV OF ALA HUNTSVILLE MECH ENGRNG DEPT W P SCHONBERG HUNTSVILLE AL 35899	1	M L ALME 2180 LOMA LINDA DR LOS ALAMOS NM 87544-2769
2	UNIV OF DAYTON RSCH INST N BRAR A PIEKUTOWSKI 300 COLLEGE PARK DAYTON OH 45469-0182	1	APPLIED RESEARCH ASSOC INC J D YATTEAU 5941 S MIDDLEFIELD RD SUITE 100 LITTLETON CO 80123
3	UNIV OF DE DEPT OF MECHANICAL ENGRNG J GILLESPIE J VINSON D WILKINS NEWARK DE 19716	2	APPLIED RESEARCH ASSOC INC D GRADY F MAESTAS SUITE A220 4300 SAN MATEO BLVD NE ALBUQUERQUE NM 87110
1	UNIV OF IL PHYSICS BUILDING A V GRANATO URBANA IL 61801	1	APPLIED RESEARCH LAB T M KIEHNE PO BOX 8029 AUSTIN TX 78713-8029
1	UNIV OF PA P A HEINEY DEPT OF PHYSICS & ASTRNMY 209 SOUTH 33RD ST PHILADELPHIA PA 19104	1	ATA ASSOCIATES W ISBELL PO BOX 6570 SANTA BARBARA CA 93111
1	UNIV OF TX DEPT OF MECHANICAL ENGRNG E P FAHRENTHOLD AUSTIN TX 78712	1	BRIGS CO J E BACKOFEN 2668 PETERSBOROUGH ST HERNDON VA 20171-2443

NO. OF COPIES	ORGANIZATION	NO. OF COPIES	ORGANIZATION
1	INTERPLAY F E WALKER 584 W TREELINE DR ALPINE UT 84004	3	LOCKHEED MARTIN MISSILE & SPACE M A LEVIN ORG 81 06 BLDG 598 M R MCHENRY T A NGO ORG 81 10 BLDG 157 111 LOCKHEED WAY SUNNYVALE CA 94088
1	ITT SCIENCES AND SYSTEMS J WILBECK 600 BLVD SOUTH SUITE 208 HUNTSVILLE AL 35802	4	LOCKHEED MISSILE & SPACE J R ANDERSON W C KNUDSON S KUSUMI 0 81 11 BLDG 157 J PHILLIPS 0 54 50 PO BOX 3504 SUNNYVALE CA 94088
1	R JAMESON 624 ROWE DR ABERDEEN MD 21001	1	LOCKHEED MISSILE & SPACE R HOFFMAN SANTA CRUZ FACILITY EMPIRE GRADE RD SANTA CRUZ CA 95060
1	KAMAN SCIENCES CORP D L JONES 2560 HUNTINGTON AVE SUITE 200 ALEXANDRIA VA 22303	1	MCDONNELL DOUGLAS ASTRONAUTICS CO B L COOPER 5301 BOLSA AVE HUNTINGTON BEACH CA 92647
7	KAMAN SCIENCES CORP J ELDER R P HENDERSON D A PYLES F R SAVAGE J A SUMMERS T W MOORE T YEM 600 BLVD S SUITE 208 HUNTSVILLE AL 35802	2	NETWORK COMPUTING SERVICES INC T HOLMQUIST G JOHNSON 1200 WASHINGTON AVE S MINNEAPOLIS MN 55415
1	D R KENNEDY & ASSOC INC D KENNEDY PO BOX 4003 MOUNTAIN VIEW CA 94040	1	PHYSICAL SCIENCES INC P NEBOLSINE 20 NEW ENGLAND BUS CTR ANDOVER MA 01810
1	LOCKHEED MARTIN ELEC & MSLS G W BROOKS 5600 SAND LAKE RD MP 544 ORLANDO FL 32819-8907	2	GD OTS D BOEKA N OUYE 400 ESTUDILLO AVE SUITE 100 SAN LEANDRO CA 94577-0205
1	LOCKHEED MARTIN MISSILE & SPACE W R EBERLE PO BOX 070017 HUNTSVILLE AL 35807	1	PRC INC J ADAMS 5166 POTOMAC DR 103 KING GEORGE VA 22485-5824

1   RAYTHEON ELECTRONIC SYSTEMS
R LLOYD
50 APPLE HILL DRIVE
TEWKSBURY MA 01876

1   ROCKWELL INTERNATIONAL
ROCKETDYNE DIVISION
H LEIFER
16557 PARK LN CIRCLE
LOS ANGELES CA 90049

1   ROCKWELL MISSILE SYS DIV
T NEUHART
1800 SATELLITE BLVD
DULUTH GA 30136

1   SAIC
M W MCKAY
10260 CAMPUS POINT DR
SAN DIEGO CA 92121

1   SHOCK TRANSIENTS INC
D DAVISON
BOX 5357
HOPKINS MN 55343

2   SOUTHERN RESEARCH INSTITUTE
L A DECKARD
D P SEGERS
PO BOX 55305
BIRMINGHAM AL 35255-5305

5   SRI INTERNATIONAL
J D COLTON
D CURRAN
R KLOOP
R L SEAMAN
D A SHOCKEY
333 RAVENSWOOD AVE
MENLO PARK CA 94025

2   TELEDYNE BROWN ENGR
J W BOOTH
M B RICHARDSON
PO BOX 070007 MS 50
HUNTSVILLE AL 35807-7007

1   ZERNOW TECHNICAL SVCS INC
L ZERNOW
425 W BONITA AVE SUITE 208
SAN DIMAS CA 91773

ABERDEEN PROVING GROUND

63   DIR USARL
AMSRL SL B
  P TANENBAUM
AMSRL SL BD
  R GROTE
  J POLESNE
AMSRL SL BE
  D BELY
AMSRL WM
  N GNIAZDOWSKI
AMSRL WM BC
  A ZIELINSKI
AMSRL WM BE S
  L HOWARD
AMSRL WM BD
  R PESCE RODRIGUEZ
  A J KOTLAR
AMSRL WM MB
  G GAZONAS
  C HOPPEL
AMSRL WM MC
  E CHIN
  J LASALVIA
AMSRL WM T
  B BURNS
  T W WRIGHT
  W GILLICH
AMSRL WM TA
  W BRUCHEY
  T HAVEL
  M BURKINS
  W A GOOCH
  T HADUCH
  E HORWATH
  D KLEPONIS
  B LEAVY
  M NORMANDIA
  J RUNYEON
  G SILSBY
AMSRL WM TB
  P BAKER
  R BITTING
  R LOTTERO
  J STARKENBERG

ABERDEEN PROVING GROUND (CONT'D)

AMSRL WM TC
 R COATES
 J BARB
 N BRUCHEY
 M FERMEN COKER
 E KENNEDY
 K KIMSEY
 L MAGNESS
 D SCHEFFLER
 S SCHRAML
 B SORENSEN
 R SUMMERS
 W WALTERS
 G RANDERS-PEHRSON LLNL
AMSRL WM TD
 S SCHOENFELD
 S R BILYK
 T W BJERKE
 D CASEM
 D DANDEKAR
 M GREENFIELD
 Y I HUANG
 H KANG
 H W MEYER
 M RAFTENBERG
 E RAPACKI
 M SCHEIDLER
 S SEGLETES (3 CPS)
 J SLATER
 T WEERISOORIYA
AMSRL WM TE
 J POWELL
 A PRAKASH

NO. OF COPIES	ORGANIZATION

2   AERONAUTICAL & MARITIME
RESEARCH LABORATORY
S CIMPOERU
D PAUL
PO BOX 4331
MELBOURNE VIC 3001
AUSTRALIA

1   DSTO AMRL
WEAPONS SYSTEMS DIVISION
N BURMAN (RLLWS)
SALISBURY
SOUTH AUSTRALIA 5108
AUSTRALIA

1   ROYAL MILITARY ACADEMY
G DYCKMANS
RENAISSANCELAAN 30
1000 BRUSSELS
BELGIUM

1   BULGARIAN ACADEMY OF
SCIENCES
SPACE RESEARCH INSTITUTE
V GOSPODINOV
1000 SOFIA
PO BOX 799
BULGARIA

1   CANADIAN ARSENALS LTD
P PELLETIER
5 MONTEE DES ARSENAUX
VILLIE DE GRADEUR PQ J5Z2
CANADA

1   DEFENCE RSCH ESTAB SUFFIELD
D MACKAY
RALSTON ALBERTA
TOJ 2NO RALSTON
CANADA

1   DEFENCE RSCH ESTAB SUFFIELD
C WEICKERT
BOX 4000 MEDICINE HAT
ALBERTA TIA 8K6
CANADA

1   DEFENCE RSCH ESTAB VALCARTIER
ARMAMENTS DIVISION
R DELAGRAVE
2459 PIE X1 BLVD N
PO BOX 8800
CORCELETTE QUEBEC GOA 1R0
CANADA

1   CEA
R CHERET
CEDEX 15
313 33 RUE DE LA FEDERATION
PARIS 75752
FRANCE

1   CEA/CESTA
A GEILLE
BOX 2 LE BARP 33114
FRANCE

5   CENTRE D'ETUDES DE GRAMAT
C LOUPIAS
P OUTREBON
J CAGNOUX
C GALLIC
J TRANCHET
GRAMAT 46500
FRANCE

6   CENTRE DE RECHERCHES
ET D'ETUDES D'ARCUEIL
D BOUVART
C COTTENNOT
S JONNEAUX
H ORSINI
S SERROR
F TARDIVAL
16 BIS AVENUE PRIEUR DE
LA COTE D'OR
F94114 ARCUEIL CEDEX
FRANCE

1   DAT ETBS CETAM
C ALTMAYER
ROUTE DE GUERRY BOURGES
18015
FRANCE

1   ETBS DSTI
P BARNIER
ROUTE DE GUERAY
BOITE POSTALE 712
18015 BOURGES CEDEX
FRANCE

1   FRENCH GERMAN RESEARCH INST
P Y CHANTERET
CEDEX 12 RUE DE I'INDUSTRIE
BP 301
F68301 SAINT LOUIS
FRANCE

5	FRENCH GERMAN RESEARCH INST H J ERNST F JAMET P LEHMANN K HOOG H F LEHR CEDEX 5 5 RUE DU GENERAL CASSAGNOU SAINT LOUIS 68301 FRANCE
1	CONDAT J KIERMEIR MAXIMILIANSTR 28 8069 SCHEYERN FERNHAG GERMANY
1	DIEHL GBMH AND CO M SCHILDKNECHT FISCHBACHSTRASSE 16 D 90552 ROETBENBACH AD PEGNITZ GERMANY
4	ERNST MACH INSTITUTE V HOHLER E SCHMOLINSKE E SCHNEIDER K THOMA ECKERSTRASSE 4 D 7800 FREIBURG I BR 791 4 GERMANY
3	FRAUNHOFER INSTITUTE FUER KURZZEITDYNAMIK ERNST MACH INSTITUT H ROTHENHAEUSLER H SENF E STRASSBURGER KLINGELBERG 1 D79588 EFRINGEN-KIRCHEN GERMANY
3	FRENCH GERMAN RESEARCH INST G WEIHRAUCH R HUNKLER E WOLLMANN POSTFACH 1260 WEIL AM RHEIN D-79574 GERMANY

2	IABG M BORRMANN H G DORSCH EINSTEINSTRASSE 20 D 8012 OTTOBRUN B MUENCHEN GERMANY
1	INGENIEURBUERO DEISENROTH AUF DE HARDT 33 35 D5204 LOHMAR 1 GERMANY
1	TU MUENCHEN E IGENBERGS ARCISSTRASSE 21 8000 MUENCHEN 2 GERMANY
1	NATIONAL GEOPHYSICAL RESEARCH INSTITUTE G PARTHASARATHY HYDERABAD 500 007 A P INDIA
1	UNIVERSITY OF ROORKEE DEPARTMENT OF PHYSICS N DASS ROORKEE 247 667 INDIA
5	RAFAEL BALLISTICS CENTER E DEKEL Y PARTOM G ROSENBERG Z ROSENBERG Y YESHURUN PO BOX 2250 HAIFA 31021 ISRAEL
1	TECHNION INST OF TECH FACULTY OF MECH ENGNG S BODNER TECHNION CITY HAIFA 32000 ISRAEL
1	IHI RESEARCH INSTITUTE STRUCTURE & STRENGTH T SHIBUE 1 15 TOYOSU 3 KOTO TOKYO 135 JAPAN

NO. OF COPIES	ORGANIZATION	NO. OF COPIES	ORGANIZATION
1	ESTEC CS D CASWELL BOX 200 NOORDWIJK 2200 AG NETHERLANDS	2	IOFFE PHYSICO TECHNICAL INSTITUTE DENSE PLASMA DYNAMICS LABORATORY E M DROBYSHEVSKI A KOZHUSHKO ST PETERSBURG 194021 RUSSIAN REPUBLIC
4	PRINS MAURITS LAB H J REITSMA E VAN RIET H PASMAN R YSSELSTEIN TNO BOX 45 RIJSWIJK 2280AA NETHERLANDS	1	IPE RAS A A BOGOMAZ DVORTSOVAIA NAB 18 ST PETERSBURG RUSSIAN REPUBLIC
1	ROYAL NETHERLANDS ARMY J HOENEVELD V D BURCHLAAN 31 PO BOX 90822 2509 LS THE HAGUE NETHERLANDS	2	LAVRENTYEV INST HYDRODYNAMICS L A MERZHIEVSKY V V SILVESTROV 630090 NOVOSIBIRSK RUSSIAN REPUBLIC
1	INSTITUTE OF CHEMICAL PHYSICS A YU DOLGOBORODOV KOSYGIN ST 4 V 334 MOSCOW RUSSIAN REPUBLIC	1	MOSCOW INST OF PHYSICS & TECH S V UTYUZHNIKOV DEPT OF COMPUTATIONAL MATHEMATICS DOLGOPRUDNY 1471700 RUSSIAN REPUBLIC
4	INSTITUTE OF CHEMICAL PHYSICS RUSSIAN ACADEMY OF SCIENCES G I KANEL A M MOLODETS S V RAZORENOV A V UTKIN 142432 CHERNOGOLOVKA MOSCOW REGION RUSSIAN REPUBLIC	1	RESEARCH INSTITUTE OF MECHANICS NIZHNIY NOVGOROD STATE UNIV A SADYRIN P R GAYARINA 23 KORP 6 NIZHNIY NOVGOROD 603600 RUSSIAN REPUBLIC
3	INSTITUTE OF MECH ENGINEERING PROBLEMS V BULATOV D INDEITSEV Y MESCHERYAKOV BOLSHOY 61 V O ST PETERSBURG 199178 RUSSIAN REPUBLIC	2	RUSSIAN FEDERAL NUCLEAR CTR VNIIEF L F GUDARENKO R F TRUNIN MIRA AVE 37 SAROV 607190 RUSSIAN REPUBLIC
1	INSTITUTE OF MINEROLOGY & PETROGRAPHY V A DREBUSHCHAK UNIVERSITETSKI PROSPEKT 3 630090 NOVOSIBIRSK RUSSIAN REPUBLIC	1	ST PETERSBURG STATE TECHNICAL UNIV FACULTY OF PHYSICS AND MECHANICS DEPT OF THEORETICAL MECHANICS ATTN A KRIVTSOV POLITECHNICHESKAYA STREET 29 195251 ST PETERSBURG RUSSIAN REPUBLIC

NO. OF COPIES	ORGANIZATION	NO. OF COPIES	ORGANIZATION
1	SAMARA STATE AEROSPACE UNIV L G LUKASHEV SAMARA RUSSIAN REPUBLIC	1	CENTURY DYNAMICS LTD N FRANCIS DYNAMICS HOUSE HURST RD HORSHAM WEST SUSSEX RH12 2DT UNITED KINGDOM
1	UNIVERSIDAD DE CANTABRIA FACULTAD DE CIENCIAS DEPARTMENTO DE FISICA APLICADA J AMOROS AVDA DE LOS CASTROS S/N 39005 SANTANDER SPAIN	5	DERA I CULLIS J P CURTIS Q13 A HART Q13 K COWAN Q13 M FIRTH R31 FORT HALSTEAD SEVENOAKS KENT TN14 7BP UNITED KINGDOM
1	DYNAMEC RESEARCH AB A PERSSON PO BOX 201 S 151 23 SODERTALJE SWEDEN	6	DEFENCE RESEARCH AGENCY W A J CARSON I CROUCH C FREW T HAWKINS B JAMES B SHRUBSALL CHOBHAM LANE CHERTSEY SURREY KT16 0EE UNITED KINGDOM
7	FOI SWEDISH DEFENCE RSCH AGENCY GRINDSJON RESEARCH CENTRE L GUNNAR OLSSON B JANZON G WIJK R HOLMLIN C LAMNEVIK L FAST M JACOB SE 147 25 TUMBA SWEDEN	1	UK MINISTRY OF DEFENCE G J CAMBRAY CBDE PORTON DOWN SALISBURY WITTSHIRE SPR 0JQ UNITED KINGDOM
2	SWEDISH DEFENCE RSCH ESTAB DIVISION OF MATERIALS S J SAVAGE J ERIKSON STOCKHOLM S 17290 SWEDEN	1	K TSEMBELIS SHOCK PHYSICS GROUP CAVENDISH LABORATORY PHYSICS & CHEMISTRY OF SOLIDS UNIVERSITY OF CAMBRIDGE CAMBRIDGE CB3 0HE UNITED KINGDOM
2	K&W THUN W LANZ W ODERMATT ALLMENDSSTRASSE 86 CH 3602 THUN SWITZERLAND	2	UNIVERSITY OF KENT PHYSICS LABORATORY UNIT FOR SPACE SCIENCES P GENTA P RATCLIFF CANTERBURY KENT CT2 7NR UNITED KINGDOM
2	AWE M GERMAN W HARRISON FOULNESS ESSEX SS3 9XE UNITED KINGDOM		

7   INSTITUTE FOR PROBLEMS IN
        MATERIALS SCIENCE
        S FIRSTOV
        B GALANOV
        O GRIGORIEV
        V KARTUZOV
        V KOVTUN
        Y MILMAN
        V TREFILOV
        3 KRHYZHANOVSKY STR
        252142 KIEV 142
        UKRAINE

1   INSTITUTE FOR PROBLEMS
        OF STRENGTH
        G STEPANOV
        TIMIRYAZEVSKAYU STR 2
        252014 KIEV
        UKRAINE